

1 Tracking millennial-scale Holocene glacial advance and  
2 retreat using Osmium isotopes: Insights from the Greenland  
3 Ice Sheet

4

5 Alan D. Rooney<sup>a,b\*</sup>, David Selby<sup>b</sup>, Jeremy M. Lloyd<sup>c</sup>, David H. Roberts<sup>c</sup>, Andreas  
6 Lückge<sup>d</sup>, Bradley B. Sageman<sup>e</sup>, Nancy G. Prouty<sup>f</sup>

7

8 <sup>a</sup>Department of Earth and Planetary Sciences, Harvard University, Cambridge, MA,  
9 02138

10 <sup>b</sup>Department of Earth Sciences, Durham University, Durham, UK, DH1 3LE

11 <sup>c</sup>Department of Geography, Durham University, Durham, UK, DH1 3LE

12 <sup>d</sup>Bundesanstalt für Geowissenschaften und Rohstoffe, Stilleweg 2, 30655 Hannover,  
13 Germany

14 <sup>e</sup>Department of Earth and Planetary Sciences, Northwestern University, 1850 Campus  
15 Drive, Evanston, IL, USA

16 <sup>f</sup>US Geological Survey, Pacific Coastal & Marine Science Center, 400 Natural Bridges  
17 Drive, Santa Cruz, CA 95060

18 \*Corresponding Author: [alanrooney@fas.harvard.edu](mailto:alanrooney@fas.harvard.edu)

19

20 **Abstract**

21 High-resolution Os isotope stratigraphy can aid in reconstructing Pleistocene ice sheet  
22 fluctuation and elucidating the role of local and regional weathering fluxes on the marine  
23 Os residence time. This paper presents new Os isotope data from ocean cores adjacent to  
24 the West Greenland ice sheet that have excellent chronological controls. Cores MSM-520  
25 and DA00-06 represent distal to proximal sites adjacent to two West Greenland ice  
26 streams. Core MSM-520 has a steadily decreasing Os signal over the last 10 kyr  
27 ( $^{187}\text{Os}/^{188}\text{Os} = 1.35 - 0.81$ ). In contrast, Os isotopes from core DA00-06 (proximal to the  
28 calving front of Jakobshavn Isbræ) highlight four stages of ice stream retreat and advance  
29 over the past 10 kyr ( $^{187}\text{Os}/^{188}\text{Os} = 2.31; 1.68; 2.09; 1.47$ ). Our high-resolution  
30 chemostratigraphic records provide vital benchmarks for ice-sheet modelers as we  
31 attempt to better constrain the future response of major ice sheets to climate change.  
32 Variations in Os isotope composition from sediment and macro-algae (seaweed) sourced  
33 from regional and global settings serve to emphasize the overwhelming effect weathering

34 sources have on seawater Os isotope composition. Further, these findings demonstrate  
35 that the residence time of Os is shorter than previous estimates of  $\sim 10^4$  yr.

## 36 **Introduction**

37 The Greenland Ice Sheet (GrIS) is the largest ice reservoir in the Arctic  
38 containing the equivalent of *c.* 7 m of global sea level and numerical modeling suggests  
39 the GrIS could contribute  $>0.5$  m of global sea level rise by A.D. 2100 (Gregory et al.,  
40 2004; Pfeffer et al., 2008). The large volumes of icebergs and meltwater delivered from  
41 the GrIS can produce major changes in ocean circulation, ecosystems and, ultimately,  
42 affect climate (McManus et al., 2004; Christoffersen and Hambrey, 2006; Raiswell et al.,  
43 2006). Direct observations of the GrIS have revealed rapid changes in mass balance on  
44 sub-decadal time scales in response to changing climate forcing (Joughin et al., 2004;  
45 Rignot and Kanagaratnam, 2006; Howat et al., 2007; Holland et al., 2008; Nick et al.,  
46 2009; Straneo et al., 2013; Khan et al., 2015). However, the drivers and mechanisms of  
47 longer-term, climatic changes to polar ice sheets are less well understood.

48 At the end of the Last Glacial Maximum (LGM) the GrIS extended onto the  
49 continental shelf of Greenland (Roberts et al., 2010; Funder et al., 2011; O’Cofaigh et al.,  
50 2013). Evidence from periglacial features, sedimentary archives, fossil foraminifera  
51 assemblages and  $\delta^{18}\text{O}$  records from benthic foraminifera suggest that the ice margin in  
52 West Greenland underwent numerous, extensive advances and retreats due to fluctuations  
53 in atmospheric and ocean temperatures during the LGM/Holocene transition and within  
54 the Holocene (Long et al., 2006; Young et al., 2011; 2013; Lane et al., 2014). In this  
55 paper we explore the duration and amplitude of these ice sheet fluctuations using  
56 nearshore sedimentary sequences where coupled sedimentological and geochemical  
57 studies can potentially elucidate ice sheet response to centennial and millennial-scale  
58 climatic forcings. In particular, we present osmium isotopic data from three sediment  
59 cores from the western Greenland margin that document rapid responses of the ice sheet  
60 to changing climate through the Holocene.

61 Radiogenic isotopes have previously been employed to assess large-scale  
62 variations in continental weathering rates related to glacial-interglacial cycles (e.g.  
63 Farmer et al., 2003; Colville et al., 2011). The Sr-Nd-Pb isotope systems have been used  
64 to evaluate changes in seawater chemistry during Pleistocene glacial-interglacial periods

65 and shown to respond to fluctuations in ice sheet mass (Blum and Erel, 1995; Farmer et  
66 al., 2003; Colville et al., 2011; Flowerdew et al., 2013; Jonkers et al., 2015). Osmium  
67 (Os) isotopes ( $^{187}\text{Os}/^{188}\text{Os}$ ) have also been used to understand the interplay between  
68 silicate weathering, and palaeoceanographic processes during the Pleistocene glacial-  
69 interglacial cycles, Late Ordovician and Neoproterozoic glacial events (Oxburgh, 1998;  
70 Peuker-Ehrenbrink and Ravizza, 2000; Williams and Turekian, 2004; Dalai et al., 2005;  
71 Dalai and Ravizza, 2006; Oxburgh et al., 2007; Paquay et al., 2009; Burton et al., 2010;  
72 Finlay et al., 2010; Paquay and Ravizza, 2012; Rooney et al., 2014).

73 For the Pleistocene glacial-interglacial cycles Os isotope data from global sites  
74 display heterogeneous profiles, which are interpreted to reflect changes in the local Os  
75 seawater composition of individual basins resulting from greater oceanographic  
76 restriction rather than changes in silicate weathering rates across the glacial-interglacial  
77 periods (Paquay and Ravizza, 2012). A similar oceanographic control on seawater  
78  $^{187}\text{Os}/^{188}\text{Os}$  compositions is observed for global sites during the ice-free Cretaceous world  
79 (c. 94 Ma, Du Vivier et al., 2014; 2015).

80 To help understand the complexities of palaeoceanography that potentially control  
81 the Os data shown for the Pleistocene glacial-interglacial cycles we investigate the use of  
82 Os isotopes to track Holocene variability of the GrIS in the Disko Bugt-Uummannaq  
83 region. This study focuses on three time-correlated sedimentary sequences: one proximal  
84 to the GrIS currently influenced by seasonal meltwater flux; one intermediate site mid-  
85 way across the continental shelf; and one in a distal setting beyond the continental shelf  
86 on the northern edge of the Labrador Sea (Fig. 1). All sites have been previously studied  
87 for their biostratigraphy, sedimentology and chronology (Lloyd et al., 2005; McCarthy,  
88 2011; Knutz et al., 2011), and are adjacent to ice sheet catchments with well-constrained  
89 glacial histories. At the LGM the GrIS extended 300 to 400 km across the continental  
90 shelf in the Uummannaq – Disko Bugt region and was grounded at the shelf edge  
91 (O’Cofaigh et al., 2013; Jennings et al., 2014). A combination of radiocarbon dating and  
92 cosmogenic radiogenic nuclide dating has been used to track ice retreat through the  
93 Uummannaq and Disko fjord systems (Lloyd et al., 2005; Young et al. 2013; O’Cofaigh  
94 et al., 2013; Roberts et al., 2013; Lane et al., 2014). By integrating the new Os isotope  
95 data with current palaeoceanographic model(s) we demonstrate the ability of Os to

96 reconstruct ice sheet fluctuations, and that oceanographic setting critically controls the  
97  $^{187}\text{Os}/^{188}\text{Os}$  composition of the seawater.

98

### 99 **Studied sites and sample material**

100 The three study sites are located along a transect from proximal to distal in  
101 relation to the present day GrIS as follows: Core DA00-06 from a proximal setting <10  
102 km from the mouth of Jakobshavn Isfjord within Disko Bugt; Core MSM-520 from an  
103 intermediary location *c.* 70 km northwest of the Nuussuaq Peninsula mid-way across the  
104 shelf within the Uummannaq fjord and; Core DA-04-31T from a distal location beyond  
105 the continental shelf *c.* 200 km southwest of Nuuk at the northern edge of the Labrador  
106 Sea (Figs. 1A, B). Hypothetically these three cores should record changing Os isotopes in  
107 different environments relative to the ice margin as all three regions are at the  
108 convergence of multiple water masses (Fig. 1) and are sourcing Os from highly variable  
109 bedrock lithologies (Table 1; Figure 2). In addition, we have sampled bedrock, other  
110 surface sediments, and algae for comparison to nearby source regions and far field areas  
111 not affected by the GrIS.

112 *Core DA00-06:* This is a 960 cm long piston core collected from a water depth of  
113 363 m by the *R/V Dana* in 2000 (Table 2). This core spans *c.* 9.0 ka based on six  
114 Accelerator Mass Spectrometry (AMS) radiocarbon dates and records deposition  
115 proximal to the mouth of the Jakobshavn Isbræ in Disko Bugt (Lloyd et al., 2005; Hogan  
116 et al., 2011; Table 2). Sediments comprise blue-grey silty organic matter-bearing clay  
117 with occasional ice rafted clasts from the base of the core up to 100 cm where there is a  
118 transition to a clast dominated organic matter-bearing sandy silt to the top of the core  
119 (Lloyd et al., 2005). The lithology and biostratigraphy are interpreted to document the  
120 retreat of Jakobshavn Isbræ across inner Disko Bugt and into Jakobshavn Isfjord. High  
121 sedimentation rates in the lower section of the core ( $13.8 \text{ mm a}^{-1}$ ) and a predominance of  
122 glaciomarine benthic foraminiferal fauna are suggestive of a still-stand in retreat as the  
123 ice stream was pinned on the sill of Jakobshavn Isfjord from 9.0 to 7.6 ka cal. BP (Figure  
124 3A; Lloyd et al. 2005). After *c.* 7.6 ka the ice stream retreated into the main fjord system  
125 and sedimentation rates fell to  $0.24 \text{ mm a}^{-1}$  for the upper 100 cm of the core with an  
126 Atlantic water influenced benthic foraminiferal assemblage dominating (Figure 3A). This

127 switch in fauna is indicative of increasing influence of the relatively warm and saline  
128 West Greenland Current at the core site from *c.* 7.6 ka (Lloyd et al., 2005). A radiocarbon  
129 date of 9.0 ka cal. BP from near the base of the core provides a minimum age constraint  
130 for deglaciation in this region of Disko Bugt (Lloyd et al., 2005).

131 *Core MSM-520:* This 1200 cm gravity core was recovered from a water depth of  
132 545 m during a cruise of the *R/V Maria S Merian* in 2007. The core records  
133 sedimentation over the last *c.* 11 ka based on 10 AMS radiocarbon dates (McCarthy,  
134 2011; Tables 2, 3). The sediments from the lower section of the core (from 990 to 879  
135 cm) are composed of rigid, blue-grey, silty organic matter-bearing clay with abundant  
136 coarse clasts. From 879 cm there is a transition to softer more clay rich sediments with  
137 scattered ice rafted clasts through the rest of the core (McCarthy, 2011). Based on the  
138 sedimentology and benthic foraminiferal assemblage the lower section of the core from  
139 990 – 879 cm has been interpreted as a subglacial till (very stiff diamicton with no  
140 foraminifera). Towards the top of this unit and at the transition to the overlying sediments  
141 benthic foraminifera are initially dominated by typical glaciomarine species (e.g.,  
142 *Elphidium excavatum f. clavata*, *Cassidulina reniforme*). The sedimentological and  
143 biostratigraphy data delineate the broad timing of the retreat of the ice stream through  
144 Uummannaq fjord with the core site being deglaciated by a minimum of 10.8 ka cal. BP  
145 (McCarthy, 2011). The benthic foraminiferal fauna record a gradual transition to a more  
146 distal glaciomarine environment by 8 ka cal. BP with the appearance of Atlantic water  
147 influenced species (e.g. *Adercotryma glomerata*, *Saccammina difflugiformis*) (McCarthy,  
148 2011), indicating the increasing influence of the West Greenland Current at the core site  
149 (Figure 3B). The biostratigraphy coupled with cosmogenic exposure ages from the  
150 Uummannaq Fjord region suggest that the ice streams had retreated to the near present-  
151 day location by *c.* 11 – 10 ka (Roberts et al., 2013; Lane et al., 2014). In summary, the  
152 sediments of core MSM-520 represent a more distal setting to the modern ice front in  
153 comparison to core DA00-06.

154 *Core DA-04-31T:* This core is a 78 cm long trigger core collected from a water  
155 depth of 2525 m during a cruise of the *R/V Dana* in 2004, adjacent to a longer piston core  
156 (878 cm long). The chronology of the main piston core was based on 12 AMS  
157 radiocarbon dates (Knutz et al., 2011). Lithostratigraphic correlations between the trigger

158 core and piston core indicate that the trigger core (78 cm) records sedimentation over the  
159 past *c.* 11 ka. Whilst this is not as accurate as the age models for the other cores it does  
160 provide strong support for the interpretation that DA-04-31T records sedimentation over  
161 the Holocene epoch. The sediments of the trigger core are composed of brown to grey  
162 silty organic matter-bearing clay with rare ice rafted clasts. The trigger core represents  
163 sedimentation in an open ocean setting, significantly beyond the continental shelf and  
164 direct influence from grounded ice. Knutz et al. (2011) identify a decreasing influence of  
165 meltwater from the retreating GrIS from *c.* 11 – 9 ka. From *c.* 9 ka the core site is more  
166 strongly influenced by a branch of the West Greenland Current that flows westward  
167 across the Davis Strait along the northern edge of the Labrador Sea (Knutz et al., 2011).

168 *Surface sediments and algae from near Greenland:* Four surface sediment  
169 samples from  $\leq 5$  cm below the seafloor were selected from locations in the Disko Bugt –  
170 Uummannaq area to characterize the modern-day seawater Os composition (MSM-340;  
171 380; 540 and Site 4; Fig. 1B). All surface sediment samples were composed of brown to  
172 grey silty organic matter-bearing clay with occasional ice rafted clasts. Three brown  
173 macro-algae (seaweed) were obtained for Os isotope analysis from the coastal regions of  
174 Qeqertarsuaq (*Ascopyllum nodosum*), Vaigat (*Laminaria digitata*) and Karrat (*Fucus*  
175 *distichus*) fjords to complement the surface sediment samples (Fig. 1A).

176 *Surface sediments and algae from far-field sites:* To provide insight into the Os  
177 composition of the Holocene ocean for sediments deposited in non-glacial settings we  
178 also present data from the Laccadive Sea (core SO93, water depth of 1688 m, 140 miles  
179 southwest of Sri Lanka and India), Mentawai Strait (core SO189, water depth of 571 m,  
180 20 miles off the coast of West Sumatra), and the Pacific Ocean (core SO161, water depth  
181 of 1001 m, 45 miles off the coast of Chile; Table 1). Lastly, we include data for three  
182 *Sargassum* seaweed samples collected from surface waters between 26 and 28°N and 87  
183 and 89°W in the Gulf of Mexico (Table 1).

184 *Greenland bedrock:* Samples representative of the most common bedrock  
185 lithologies in the Disko Bugt – Uummannaq region were analyzed for their Re and Os  
186 elemental abundances and isotopic compositions in order to trace the sources of Os that  
187 determine the isotopic signal of seawater at the core sites (Fig. 1A). These lithologies are  
188 as follows; Archean tonalitic orthogneiss sampled from the island of Salliaruseq Storøen

189 (70°40'05"N, 51°33'08"W), and Paleoproterozoic metagreywacke from the Nûkavsak  
190 Formation (71°31'18"N, 52°57'32"W) of the Karrat Group. A sample of basalt was taken  
191 from the Vaigat Formation on the Svartenhuk peninsula (71°31'10"N, 55°17'29"W).

192

## 193 **Methods**

### 194 *TOC and Re-Os Analytical Protocols*

195 Bedrock samples were cut and polished to remove any saw markings and together  
196 with soft sediment from sampled cores, dried at 60 °C for 48 hrs. Seaweed samples were  
197 rinsed with milliQ and dried at 60 °C for 24 hrs. Approximately 30 to 50 g for each rock  
198 or sediment sample was powdered in a Zirconia ceramic dish using a shatterbox to a fine  
199 (~30 µm) powder. For seaweed, a frond was ground in agate to a fine powder (~100 µm).

200 Powdered core samples were analyzed for weight percent concentration of total  
201 carbon (TC) by combustion at 950 °C in a stream of O<sub>2</sub>, and total inorganic carbon (TIC)  
202 by acidification with 10% phosphoric acid. Sample carbon converted to CO<sub>2</sub> by each  
203 preparation method is quantified by coulometric titration (Huffman, 1977; Engleman et  
204 al., 1985). Analysis of standards and replicates indicates average uncertainty less than  
205 ±1%. Total organic carbon (TOC) is calculated as the difference between wt.% TC and  
206 TIC. The TIC value is converted to wt.% calcium carbonate by stoichiometric calculation  
207 (wt.% TIC x 8.333), which assumes negligible quantities of inorganic carbon present as  
208 minerals other than calcium carbonate.

209 Rhenium and osmium abundances and isotope compositions were determined  
210 using isotope dilution negative thermal ionization mass spectrometry at the Durham  
211 University Laboratory for Source Rock and Sulfide Geochronology and Geochemistry  
212 using carius-tube digestion with solvent extraction, micro-distillation, and anion  
213 chromatography methods (Selby and Creaser, 2003; Cumming et al., 2013; Prouty et al.,  
214 2014).

215 In addition to being siderophilic and chalcophilic, Re and Os are organophilic.  
216 Rhenium and osmium in the water column are complexed to organic matter and with  
217 burial become preserved in organic-rich sediments (Ravizza and Turekian, 1989). In  
218 organic matter the Re and Os are predominantly bound to the kerogen fraction (Rooney et  
219 al., 2012). This study utilized the Cr<sup>VI</sup>O<sub>3</sub>- 4N H<sub>2</sub>SO<sub>4</sub> digestion technique, which has been

220 shown to significantly limit the contribution of detrital Re and Os even in low TOC, and  
221 Re and Os bearing organic-rich rocks (e.g., Selby and Creaser, 2003; Kendall et al., 2004;  
222 Rooney et al., 2011; Kendall et al., 2013). Accurate and precise depositional Re-Os age  
223 determinations and Os isotope compositions of the water column contemporaneous with  
224 sediment deposition have been obtained from sedimentary rocks with as little as 0.5 wt.%  
225 TOC, but also as low as 0.1 wt.% TOC (Rooney et al., 2011; 2014; Harris et al., 2013;  
226 Selby et al., 2013; Kendall et al., 2013; Du Vivier et al., 2014; 2015; Rooney et al., 2014;  
227 Sperling et al., 2014). Average TOC values of the sample sets of this study are as  
228 follows: 0.27 wt.% for core DA00-06; 1.25 wt.% for core MSM-520; and 0.22 wt.% for  
229 core DA-04-31T (Table 4). These values are higher than the average of 0.1 wt.% reported  
230 by Sperling et al. (2014) suggesting that the Re-Os data presented here (generated using  
231 the  $\text{Cr}^{\text{VI}}\text{O}_3\text{-H}_2\text{SO}_4$  technique) is a faithful record of hydrogenous Re and Os and not  
232 detrital Os from silicate minerals and thus suitable for assessing the Holocene  $^{187}\text{Os}/^{188}\text{Os}$   
233 seawater record.

234 For all samples between 0.2 and 1.6 g of powder was digested in a carius-tube  
235 with a known amount of a  $^{185}\text{Re}\text{-}^{190}\text{Os}$  tracer solution with an acid medium (8 mL of 0.25  
236 g/g  $\text{Cr}^{\text{VI}}\text{O}_3\text{-}4\text{N H}_2\text{SO}_4$  for sediments; 9 mL of 1:2 mix of 11 N HCl: 15.5 N  $\text{HNO}_3$  for  
237 bedrock and seaweed samples) at 220 °C for 48 hrs. Osmium was isolated and purified  
238 from the acid medium using  $\text{CHCl}_3$  solvent extraction into HBr, and then micro-  
239 distillation. Rhenium was isolated and purified using  $\text{NaOH-C}_3\text{H}_6\text{O}$  solvent extraction  
240 and anion chromatography. The isolated Re and Os fractions were loaded onto Ni and Pt  
241 filaments respectively, for their isotopic composition determination using a  
242 ThermoElectron TRITON mass spectrometer. Rhenium and Os isotope compositions  
243 were obtained using Faraday collectors and the secondary electron multiplier,  
244 respectively. Full analytical procedural blanks for this study are  $13.2 \pm 0.1$  pg for Re;  
245  $0.13 \pm 0.13$  pg for Os with an  $^{187}\text{Os}/^{188}\text{Os}$  of  $0.264 \pm 0.456$  (1SD, n=2 for  $\text{Cr}^{\text{VI}}\text{O}_3\text{-H}_2\text{SO}_4$ ),  
246 and  $1.7 \pm 0.04$  pg for Re;  $0.13 \pm 0.08$  pg for Os with an  $^{187}\text{Os}/^{188}\text{Os}$  of  $0.410 \pm 0.509$   
247 (1SD, n=2 for  $\text{HCl:HNO}_3$ ). Calculated uncertainties include those associated with mass  
248 spectrometer measurements, blank abundance and composition, reproducibility of  
249 standard Re and Os isotope values and spike calibration. In-house standard solutions of  
250 Re and Os (DROsS) yield an average  $^{185}\text{Re}/^{187}\text{Re}$  value of  $0.59806 \pm 0.00144$  (1SD,



251 n=257), and  $^{187}\text{Os}/^{188}\text{Os}$  of  $0.10693 \pm 0.000041$  (1SD, n=178), respectively, which is  
252 identical, within uncertainty to the previously published values (Nowell et al., 2008;  
253 Rooney et al., 2010). Based on the reproducibility of an organic-rich sedimentary  
254 reference sample, SDO-1, we consider only variations in  $^{187}\text{Os}/^{188}\text{Os} \geq 0.04$  between  
255 samples to be related to geological processes (Du Vivier et al., 2014; 2015).

256

## 257 **Results**

258

### 259 *Total Organic Carbon, and Rhenium and Osmium abundances*

260 All Holocene sediments analyzed in this study are characterized as organic-  
261 bearing silty-clay. Total organic carbon (Table 4) values for all samples from the DA-04-  
262 31T core are variable, ranging from a low of 0.07 wt.% at the base of the core to the  
263 highest value at the core top of 0.35 wt.%. The average TOC value for all samples from  
264 the MSM-520 core is  $1.25 \pm 0.26$  (1SD) wt.%, ranging from 0.86 to 1.63 wt.%. Values  
265 tend to increase up core. For DA00-06 TOC values are very low for the lower section of  
266 the core (ranging from 0.02 – 0.16 wt.% from 940 – 150 cm). Values then increase to  
267 0.31 – 0.81 wt.% from 110 – 10 cm (Table 4). Two surface sediment spot samples have  
268 values of 0.14 (Site 4) and 1.77 (MSM-340) wt.% TOC (Table 1). Total organic carbon  
269 for open ocean samples have similar to slightly higher abundances (TOC = 1.5 to 3.2  
270 wt.%; Table 1).

271 Rhenium and osmium elemental abundances of all Holocene organic-bearing  
272 sedimentary samples of this study range between 0.4 and 25.7 ng/g for Re, and 36.5 and  
273 353.5 pg/g for Os. The crustal lithologies gneiss, metagreywacke, and basalt have  
274 abundances of 0.004, 0.035, and 0.2 ng/g Re, and c. 6, 1.6 and 19 pg/g Os, respectively.  
275 The seaweed samples contain between 1.3 to 22.0 ng/g Re and 12.6 to 14.1 pg/g Os,  
276 respectively.

277

### 278 *Osmium isotope ( $^{187}\text{Os}/^{188}\text{Os}$ ) compositions*

279 The sampled crustal units of the Disko Bugt area have moderate to highly  
280 radiogenic  $^{187}\text{Os}/^{188}\text{Os}$  compositions from 0.44 to 2.82. Similar to these values, surface  
281 samples and seaweed of the Disko Bugt area have  $^{187}\text{Os}/^{188}\text{Os}$  compositions that range

282 between 0.48 and 2.62. In contrast to highly variable Os compositions of the surface  
283 samples of Disko Bugt area, three surface samples from the Laccadive Sea, Mentawai  
284 Strait, and Pacific Ocean have values of 1.06, 1.02 and 1.05, respectively. These values  
285 are comparable to seaweed collected from surface waters between 26 and 28°N and 87  
286 and 89°W in the Gulf of Mexico ( $^{187}\text{Os}/^{188}\text{Os}$  compositions from 1.03 to 1.06; Table 1).

287 Core DA04-31T records relatively constant  $^{187}\text{Os}/^{188}\text{Os}$  compositions ( $1.02 \pm$   
288  $0.12$ ; 1SD,  $n=8$ ) throughout the core (Fig. 3C). Core MSM-520 shows a more constant  
289 trend to less radiogenic  $^{187}\text{Os}/^{188}\text{Os}$  compositions, decreasing from 1.35 to 0.81 through  
290 the interval *c.* 11 to 0.3 ka cal. BP (Fig. 3B). Core DA00-06 records the most radiogenic  
291 Os compositions with a general trend towards less radiogenic values up core ( $^{187}\text{Os}/^{188}\text{Os}$   
292 from 2.41 to 1.34). However, in detail, four zones can be identified based on the Os  
293 compositions (Fig. 3A). Zone 1 from *c.* 9.0 – 8.0 ka cal. BP shows a gradual reduction in  
294  $^{187}\text{Os}/^{188}\text{Os}$  composition from 2.41 to 2.22; Zone 2 from *c.* 8.0 – 7.78 ka cal. BP shows a  
295 sharp reduction in  $^{187}\text{Os}/^{188}\text{Os}$  values ranging from 1.66 to 1.71; Zone 3 from *c.* 7.78 –  
296 7.50 ka cal. BP shows an increase in  $^{187}\text{Os}/^{188}\text{Os}$  values ranging from 2.02 to 2.19 and;  
297 Zone 4 from 7.50 ka cal. BP to present shows an abrupt decline to  $^{187}\text{Os}/^{188}\text{Os}$  values  
298 averaging 1.55 (Fig. 3A).

299

## 300 Discussion

301

### 302 *Consistent records of Os composition in far field sites*

303 The canonical value of present day oceanic  $^{187}\text{Os}/^{188}\text{Os}$  value of 1.06 (1.04 for the  
304 North Atlantic and Central Pacific; 1.06 for the Eastern Pacific and Indian Ocean) was  
305 from direct analyses of seawater and scrapings of hydrogenetic Fe-Mn crusts (Peucker-  
306 Ehrenbrink and Ravizza, 2012 and references therein; Gannoun and Burton, 2014 and  
307 references therein). The  $^{187}\text{Os}/^{188}\text{Os}$  values from our surface sediment samples from three  
308 non-glacially influenced ocean sites show similar values (Laccadive Sea, 1.06; Mentawai  
309 Strait, 1.02; Pacific Ocean, 1.05; Table 1). From these same sites, samples taken at *c.* 10  
310 ka have identical Os values, within uncertainty, to those at the surface (Fig. 2). This  
311 indicates that in far-field sites, seawater Os compositions are stable over kyr timescales  
312 and are reliably recorded in surface sediments. We also note that the  $^{187}\text{Os}/^{188}\text{Os}$

313 composition for three open-ocean floating seaweeds from the Gulf of Mexico ( $1.05 \pm$   
314  $0.01$ ; Table 1; Fig. 2), are identical, within uncertainty of published values, indicating that  
315 seaweed directly records the Os isotope composition of seawater.

316

#### 317 *Surface sediments in near-field sites*

318 In comparison to the far field sites, surface sediment samples from four sites  
319 within the Disko Bugt – Uummannaq region possess highly variable  $^{187}\text{Os}/^{188}\text{Os}$   
320 compositions ( $0.48$  to  $2.62$ ; Table 1; Fig. 2). Surface samples from MSM-540 (100 km  
321 west of Disko Island) and MSM-340 (80 km south-west of Disko Bugt), and seaweed  
322 from Qeqertarsuaq and Vaigat possess  $^{187}\text{Os}/^{188}\text{Os}$  values close to open ocean seawater  
323 ( $0.98 \pm 0.01$ ;  $1.13 \pm 0.01$ ,  $0.96 \pm 0.13$ ;  $0.91 \pm 0.11$ , respectively; Table 1). In contrast,  
324 surface samples from Site 4, the most proximal location to the Jakoshavn Isbræ, MSM-  
325 380 (proximal to Disko Island and Nuussuaq which are comprised solely of Paleocene  
326 tholeiitic and picritic lavas), and seaweed from the mid-point of Karrat Fjord (adjacent to  
327 Karrat Group metasediments) have markedly different  $^{187}\text{Os}/^{188}\text{Os}$  values ( $2.62 \pm 0.05$ ,  
328  $0.50 \pm 0.03$ ,  $1.89 \pm 0.24$ , respectively; Table 1).

329 As such, these  $^{187}\text{Os}/^{188}\text{Os}$  data indicate that the Os isotope composition of  
330 sediments and seaweed from more proximal coastal areas and more distal ocean areas are  
331 strongly controlled by regional variations in the Os flux into the ocean; a conclusion  
332 consistent with previous Os isotope studies of glacially-influenced marine strata (Paquay  
333 and Ravizza, 2012). Further, the marine residence time of Os, that is, the amount of Os  
334 dissolved in seawater divided by the sum of input and output fluxes, in these regions will  
335 be considerably shorter than the canonical value of  $c. 10^4$  yr.

336 Site 4 has an  $^{187}\text{Os}/^{188}\text{Os}$  value similar to the sampled Archean gneiss ( $2.62$  vs.  
337  $2.82$ ), which is the predominant bedrock source of Os from Jakoshavn Isbræ. In contrast,  
338 the surface sample from MSM-380 has an  $^{187}\text{Os}/^{188}\text{Os}$  composition ( $0.49$ ) that is less  
339 radiogenic than determined for our basalt sample ( $c. 1.3$ ), which is from the southwest  
340 coast of Svartenhuk. However, picrites from Disko Island typically have  $^{187}\text{Os}/^{188}\text{Os}$   
341 values of  $c. 0.13 - 0.14$ , and elevated Re and Os elemental abundances (up to  $0.8$  and  $3.4$   
342 ng/g, respectively), which suggest the magma originated from a relatively  
343 uncontaminated mantle source (e.g., Schaefer et al., 2000). As such, the present day

344 seawater Os value recorded at MSM-380 may represent Os sourced from the  
345 unradiogenic Os-bearing Paleocene ultramafic-mafic units of Disko Island and Nuussuaq,  
346 and radiogenic Os from the mainland gneiss. Our basalt Re-Os data is supportive of  
347 previous models suggesting that parts of the Paleocene magma system assimilated local  
348 Cretaceous sediments during eruptions (Goodrich and Patchett, 1991; Ulff-Møller, 1990;  
349 Schaefer et al., 2000), which we further demonstrate here using Os isotopes (Table 1).  
350 Lastly, seaweed from Karrat Fjord is significantly more radiogenic than the Karrat Group  
351 metagreywacke ( $^{187}\text{Os}/^{188}\text{Os} = 1.89$  and  $0.44$ , respectively), suggesting a strong flux of  
352 Os from the Archean gneiss in the Karrat Fjord.

353 Variations in the general pattern of  $^{187}\text{Os}/^{188}\text{Os}$  values between core sites reflect  
354 site proximity to differing sources of Os. Sediment from core DA00-06 (a proximal  
355 location to Jakobshavn Isbræ and in a region Archean gneiss with a modern-day  
356  $^{187}\text{Os}/^{188}\text{Os}$  value of  $2.82$ ) is more radiogenic on average than sediments from the MSM-  
357 520 core ( $0.73 - 1.35$ ) and DA-04-31T core ( $0.84 - 1.19$ ). In contrast, values from the  
358 far-field core DA04-31T are very similar to background open ocean values ( $^{187}\text{Os}/^{188}\text{Os} =$   
359  $1.06$ ). The moderately radiogenic Os isotope values from core MSM-520 most likely  
360 reflect the abundance of relatively unradiogenic bedrock in the catchment area (a  
361  $^{187}\text{Os}/^{188}\text{Os}$  value of  $0.44$  from the Paleoproterozoic metagreywacke and *c.*  $1.3$  from the  
362 Paleocene basalt).

363

#### 364 *Tracking GrIS advance and retreats using seawater Os isotope composition*

365 Trends in Os isotopes at near-ice sites can be compared to their known glacial  
366 histories. At the LGM the GrIS extended  $300$  to  $400$  km across the continental shelf in  
367 the Disko Bugt – Uummannaq region and was grounded at the shelf edge (O’Cofaigh et  
368 al., 2013; Jennings et al., 2014). Radiocarbon dated sediment cores indicate that the  
369 western ice margin retreated asynchronously from the shelf edge in the Uummannaq fjord  
370 area compared to Disko Bugt. The ice sheet began retreating from the Uummannaq fjord  
371 area *c.*  $14.8$  ka (Jennings et al., 2014). The retreat can then be traced using cosmogenic  
372 radiogenic nuclide dating to Ubekendt Ejland within the main part of Uummannaq fjord  
373 by  $12.4$  ka cal. BP, with rapid disintegration and retreat of the ice margin into the inner  
374 fjord by *c.*  $11 - 8.7$  ka (Roberts et al., 2013).

375 The Os isotope record for core MSM-520 records a steady decrease in Os values  
376 ( $^{187}\text{Os}/^{188}\text{Os} = 1.35 - 0.81$ ) from 9 – 0 ka. These generally less radiogenic Os values  
377 suggest a stronger influence of Os from the surrounding basaltic Paleocene lava flows  
378 and Paleoproterozoic metasediments ( $^{187}\text{Os}/^{188}\text{Os}$  values of 1.31 and 0.44, respectively,  
379 Table 1) and also from less radiogenic open ocean sources ( $^{187}\text{Os}/^{188}\text{Os}$  values of 1.06).  
380 The most radiogenic Os values come from the base of MSM-520 at *c.* 11 ka ( $^{187}\text{Os}/^{188}\text{Os}$   
381 = 1.35, Fig. 3B). This section of the core is dominated by a glaciomarine foraminiferal  
382 fauna and is deposited just above sediment interpreted as a subglacial till (McCarthy,  
383 2011). Taken together, these results indicate that seawater in the Uummannaq Fjord  
384 system was influenced predominantly by the input of glacially eroded material from a  
385 proximal calving margin. The steady decline in  $^{187}\text{Os}/^{188}\text{Os}$  values (1.35 to 0.81; Fig. 3B)  
386 up-core in MSM-520 is interpreted to be a consequence of the rapidly retreating  
387 Uummannaq ice stream reducing the influence of radiogenic, continentally-sourced Os  
388 reaching this location. This interpretation agrees with sedimentology and foraminiferal  
389 biostratigraphy from MSM-520 (McCarthy, 2011) and ice stream reconstructions from  
390 cosmogenic radionuclide dating of the surrounding area which clearly show ice retreat to  
391 the inner shelf/coastal fjords by *c.* 11 ka (Roberts et al., 2013; Lane et al., 2014).  
392 Furthermore, by *c.* 8 ka the increase in abundance of Atlantic water foraminifera  
393 indicates a well-established West Greenland Current implying that water masses in the  
394 Uummannaq Fjord system were connected to the open ocean, and that sediment flux from  
395 the ice margin had declined considerably (McCarthy, 2011). As such, the steady decrease  
396 in Os values through core MSM-520 also suggest a decrease in glacially eroded  
397 radiogenic material during the Holocene that we interpret to be related to the retreat of  
398 the calving ice margin (Fig. 3B). From *c.* 6 ka foraminifera data suggest that a modern  
399 oceanographic circulation pattern had began to dominate in the Disko Bugt –  
400 Uummannaq fjord area (Perner et al., 2013). Closely matching this interpretation are the  
401 extremely similar  $^{187}\text{Os}/^{188}\text{Os}$  compositions ( $0.83 \pm 0.03$ ) from 4.4 ka cal. BP to the core  
402 top. The slightly less radiogenic compositions of these upper core samples is likely  
403 related to an increase in the flux of unradiogenic Os from the Paleocene lavas, which  
404 dominate the coastline.

405 In the Disko Bugt region, retreat from the shelf edge started slightly later than at  
406 Uummannaq, beginning at 13.8 ka cal. BP (O’Cofaigh et al., 2013). This ice margin  
407 retreated across the shelf to a position just west of the entrance to Disko Bugt by *c.* 12.0  
408 ka, with evidence for a minor advance followed by rapid retreat during the Younger  
409 Dryas (O’Cofaigh et al., 2013). The ice margin then retreated through Disko Bugt  
410 reaching the inner bay by 10.2 ka cal. BP followed by marked standstills at 9.3 and 8.2 ka  
411 cal. BP. The ice reached the present day ice margin by 7.6 – 6.5 ka cal. BP (Lloyd et al.,  
412 2005; Long et al., 2006; Hogan et al., 2011).

413 Sediment from core DA00-06 (a proximal location to Jakobshavn Isbræ and in a  
414 region dominated by Archean gneiss with a modern-day  $^{187}\text{Os}/^{188}\text{Os}$  value of 2.82; Figs.  
415 1A, 2) is more radiogenic on average than sediments from the MSM-520 core (0.73 –  
416 1.35) and DA-04-31T core (0.84 – 1.19). Furthermore, given the proximity of DA00-06  
417 to Jakobshavn Isbræ and this relatively restricted embayment we suggest that the Os  
418 residence time in this area of West Greenland is considerably shorter than that of the  
419 open-ocean value ( $10^3$  vs.  $10^4$  yr). As a result of this shortened residence time, the Os  
420 isotope profile of core DA00-06 will record changes in Os isotope composition with a  
421 delay of *c.* 500 - 1000 yr. Values from core DA04-31T are very similar to background  
422 open-ocean values ( $^{187}\text{Os}/^{188}\text{Os} = 1.06$ ) suggesting this site was not affected by Holocene  
423 variations in ice sheet advance and retreat and that the residence time of Os is similar to  
424 the open ocean canonical *c.*  $10^4$  yr. However, there are trends that can be identified from  
425 the two glacial proximal cores reflecting changes in sources and delivery of Os through  
426 the Holocene connected to the advance and retreat of the GrIS.

427 At present, core site DA00-06 is proximal to the calving margin of Jakobshavn  
428 Isbræ, a major ice stream draining the GrIS, and the core sediments are strongly  
429 influenced by radiogenic meltwater from the ice sheet. The basal section of core DA00-  
430 06 (960 – 120 cm) records a brief (<2000 years) interval of rapid sedimentation (13.8 mm  
431  $\text{a}^{-1}$ ) from Jakobshavn Isbræ when it was grounded at the mouth of Jakobshavn Isfjord  
432 (Lloyd et al., 2005). In general, as the  $^{187}\text{Os}/^{188}\text{Os}$  values through this core are relatively  
433 high (1.34 – 2.41), we surmise that this reflects a dominant influence of meltwater  
434 carrying glacially eroded rock flour from the highly radiogenic Archean gneiss typical for  
435 this region (*c.* 2800 Ma gneiss  $^{187}\text{Os}/^{188}\text{Os} = 2.82$ ; Table 1). However, upon closer

436 examination of the core, four zones of varying Os isotopes can be identified (Fig. 3A;  
437 Table 4). The extremely radiogenic Os values ( $^{187}\text{Os}/^{188}\text{Os} = 2.41, 2.29, 2.22$ ) of Zone 1  
438 (9.0 – 8.0 ka cal. BP) reflect the strong influence of sediment-laden meltwater sourced  
439 from the proximally grounded Jakobshavn Isbræ. This agrees with the sedimentology and  
440 benthic foraminiferal assemblage; glaciomarine fauna (Fig. 3A) such as *Elphidium*  
441 *excavatum f. clavata*, *Cassidulina reniforme* and *Stainforthia feylingi* (Lloyd et al., 2005).  
442 We hypothesize this highly radiogenic Os signal from Zone 1 is indicative of an Os flux  
443 sourced from Archean crustal rocks when the ice stream calving margin stabilised and re-  
444 advanced at the mouth of the Isfjord between c. 10.3 and 8.2 ka (Long and Roberts, 2003;  
445 Long et al., 2006; Young et al., 2013). The markedly lower Os isotope values  
446 ( $^{187}\text{Os}/^{188}\text{Os} = 1.68, 1.71, 1.66$ ) of Zone 2 (8.0 – 7.78 ka cal. BP) are suggestive of a  
447 reduction in the flux of radiogenic rock flour to the core site. We suggest that this results  
448 from a reduction in meltwater derived glacial rock flour caused by ice margin retreat after  
449 the 8.2 ka re-advance event (Young et al, 2013). However, the foraminiferal fauna do not  
450 show any major change; the assemblage is still dominated by proximal glaciomarine  
451 species. The decrease in Os could therefore be due to a subtle shift in sediment or  
452 meltwater flux that is not registered in the foraminifera fauna (Fig. 3A). The increase in  
453 Os isotope values ( $^{187}\text{Os}/^{188}\text{Os} = 2.06, 2.08, 2.02, 2.19$ ) during Zone 3 (7.78 – 7.5 ka cal.  
454 BP) we suggest represents a return to conditions similar to Zone 1 – a finding also  
455 supported by the glaciomarine foraminifera assemblage. This increase in Os isotope  
456 values could result from greater sediment flux due to ice stream stabilization at the  
457 eastern end of the Isfjord, or a minor re-advance, but cosmogenic exposure ages suggest  
458 the ice was c. 25 to 30 km east of its 8.2 ka position by this time (Young et al., 2013).  
459 The alternative explanation is either an increase in meltwater or ice rafted debris delivery  
460 to the core site, which could correlate with increased surface ablation, run-off and calving  
461 due to increased air temperatures during the Holocene Thermal Maximum (Carlson and  
462 Winsor, 2012). There is an abrupt drop in  $^{187}\text{Os}/^{188}\text{Os}$  values from 2.19 to 1.54 at the  
463 transition from Zone 3 to Zone 4 (Fig. 3A). This final shift occurs at 7.5 ka cal BP; Os  
464 values then remain less radiogenic through to the top of the core (112 cm). This coincides  
465 with a significant shift in foraminiferal fauna with relatively warmer Atlantic water fauna  
466 (indicating a stronger influence from the West Greenland Current) replacing the

467 glaciomarine fauna (Fig. 3A). This shift is likely to be a response to the retreat of the  
468 calving front to a distal location up to 20 km inboard of the present ice margin (i.e.  
469 Holocene minimum position; Funder et al; 2011; Hogan et al., 2011; Young et al., 2013).

470 In summary, the pronounced decline in Os isotope values in core DA00-06  
471 resulted from decreasing volumes of meltwater and glacially eroded rock flour as the  
472 calving margin of the Jakobshavn Isbræ retreated from the mouth of Jakobshavn Isfjord  
473 to its present day location *c.* 50 km further from the core site during the Holocene. The  
474 trends in the Os data demonstrate a nuanced pattern of ice margin retreat, re-advance and  
475 standstill, broadly correlative with recent onshore deglacial histories (Long et al., 2006;  
476 Young et al., 2013). However, those trends contrast somewhat with offshore  
477 sedimentological and biostratigraphic evidence, which may not capture subtle shifts in  
478 sediment and meltwater flux (Lloyd et al., 2005).

479 Core DA04-31T located *c.* 200 km southwest of Nuuk beyond the continental  
480 shelf (2525 m water depth) records open ocean sedimentation for the entire Holocene  
481 epoch (Knutz et al., 2011). Samples throughout the core have broadly similar  $^{187}\text{Os}/^{188}\text{Os}$   
482 values ( $1.02 \pm 0.12$ ) with no discernable trend, indicating a minimal influence from the  
483 GrIS in contrast to cores MSM-520 and DA00-06. The DA04-31T core Os values are  
484 similar to values for other global sites and present day seawater, especially that of the  
485 North Atlantic (Paquay and Ravizza, 2012 and references therein; Gannoun and Burton,  
486 2014 and references therein; Figs. 2, 3C). The small deviations ( $\leq 4\%$ ) from the canonical  
487 seawater  $^{187}\text{Os}/^{188}\text{Os}$  value of 1.06 may relate to site-specific differences in  
488 oceanographic currents and relevant sources of Os (Paquay and Ravizza, 2012).

489 The data presented here cover a geographical transect from proximal to distal  
490 glacial setting and also temporally from proximal to distal glaciomarine conditions linked  
491 to the retreat of major ice streams. We show that Os isotopic signatures can differentiate  
492 between proximal glaciomarine settings and more distal open ocean settings. We also  
493 show that the isotopic signature can identify shifts in the flux of radiogenic glacially-  
494 eroded material and can be used to interpret the relative advance and retreat of marine  
495 terminating ice stream margins.

496

497 *Implications for seawater heterogeneity and ephemeral Os isotope compositions*



498 Previous Os isotope studies tried to provide records of variations in the intensity  
499 of continental weathering on millennial timescales (Sharma et al., 1997; Levasseur et al.,  
500 1998; Woodhouse et al., 1999). Integral to these studies is an accurate understanding of  
501 the marine residence time of Os. Constraining the residence time of Os in the oceans is  
502 challenging, primarily due to its extremely low abundance (*c.* 10 pg/kg; Gannoun and  
503 Burton, 2014) although it is thought to be an order of magnitude longer than the mixing  
504 time of the oceans, yet significantly shorter than Sr (*c.*  $10^4$  vs.  $10^6$  yr; cf. Oxburgh, 1998;  
505 Levasseur et al., 1999). The shorter residence time estimates are supported by  
506 documented heterogeneities in the modern-day Os seawater composition (Peucker-  
507 Ehrenbrink and Ravizza, 2000; Chen and Sharma, 2009; Gannoun and Burton, 2014).  
508 The diverse Os values of this study further demonstrate that seawater Os isotope  
509 composition is strongly controlled by the oceanographic setting (Paquay and Ravizza,  
510 2012; Du Vivier et al., 2014; 2015).

511 A lack of absolute constraints for the fluxes of Os from the mainland, Disko  
512 island, the volume (and seasonal volume changes) of water, salinity changes (thus likely  
513 changes in seasonal behavior of Os), and sedimentation rates within Disko Bugt hinder  
514 attempts to generate a complete model of Os isotope variations for this region. However,  
515 the Os isotope data presented in Figure 4 indicates that Os variations seen in the west  
516 Greenland samples can be partially explained as the result of physical mixing between  
517 different proportions of isotopically distinct lithogenic material. However, this can only  
518 explain mixing in the water column and cannot account for the biological uptake of Os  
519 (and Re) in macro-algae (Fig. 4; Table 2). Surface sediment samples proximal to the west  
520 Greenland margin form a well defined physical mixing trend that is bounded by bedrock  
521 samples, especially if the high concentration and low  $^{187}\text{Os}/^{188}\text{Os}$  picritic basalts reported  
522 by Schaefer et al. (2000) are included with the three bedrock lithologies investigated here  
523 (not shown on Fig. 4; Table 2).

524 Core DA00-06 shows significant, rapid changes (*c.*  $10^3$  yr) in the Os composition  
525 of seawater. Previous estimates of the residence time of Os in seawater are significantly  
526 greater (e.g.,  $\geq 50$  kyr; Oxburgh, 2001; Peucker-Ehrenbrink and Ravizza, 2012 and  
527 references therein) than the temporal changes observed here. During the Holocene epoch  
528 unradiogenic Os inputs directly from magmatic, hydrothermal and extra-terrestrial

529 sources can be considered constant and thus the Os isotope compositions of the studied  
530 sites herein are explicitly modulated by silicate weathering of the continental lithologies  
531 by the GrIS as discussed above. To explain the rapid changes in Os isotope composition  
532 recorded in these samples the Os residence time must be on the order of *c.*  $10^3$  yr. To  
533 shorten the residence time inputs must be changing during deglacial/glacial events, and/or  
534 have changing Os isotope composition of the inputs (Oxburgh, 2001).

535

## 536 **Conclusions**

537 The Os isotope compositions presented here along with paleoceanographic data  
538 demonstrate the ability to identify shifts in the flux of radiogenic glacially eroded  
539 material that can be used to track ice sheet advance and retreat patterns. Application of  
540 Os isotope stratigraphy in core DA00-06 reveals that the ocean – calving margin interface  
541 of the Jakobshavn Isbræ has a more complex history than was previously recorded by the  
542 biostratigraphy. Our Os isotope data yields four zones that mark oscillation of the  
543 Jakobshavn Isbræ calving margin during the Holocene that broadly correlate with the  
544 known deglacial history of the ice stream. These data highlight the potential for Os  
545 isotopic signatures to identify shifts in the flux of glacially derived material and  
546 ultimately better decode the dynamic behaviour of marine terminating ice streams at  
547 millennial timescales.

548 Our Os isotope values for three seaweeds from the Gulf of Mexico are identical,  
549 within uncertainty, of published seawater values, indicating that seaweed directly records  
550 the Os isotope composition of seawater. These novel isotope data yield insights into the  
551 complexation behaviour of Re and Os into organic matter and provide further context for  
552 the application of Re and Os as redox state tracers in ancient sedimentary successions.  
553 The Os isotopic profiles from the three cores presented here reveal that seawater Os  
554 composition is strongly controlled by the oceanographic setting in terms of the proximity  
555 to weathering sources and large-scale oceanic currents. Additionally, this study shows  
556 that ephemeral changes (*c.*  $10^3$  yr) in the Os composition of seawater can be identified  
557 which has implications for our understanding of the residence time of Os in the modern  
558 ocean.

559

560 **Acknowledgements**

561 We thank Barbara Stroem-Baris, Antony Long and Sarah Woodroffe for seaweed  
562 samples and Brice Rea and Tim Lane for assistance in collecting bedrock samples. We  
563 acknowledge the Bundesministerium fuer Bildung und Forschung (BMBF, Bonn) for  
564 funding the SO139 (03G01390A) and SO130 (03G0130A) cruises. This paper benefited  
565 from constructive criticisms from Greg Ravizza and Bernhard Peucker-Ehrenbrink and  
566 valuable discussions with Francis Macdonald, Sierra Petersen and Alice Doughty. An  
567 anonymous reviewer and editor Neil Glasser are also thanked for improving this  
568 manuscript.

569

570 **Figure captions:**

571 **Figure 1.** Location maps. **(A)** Map showing location of Greenland related sediment,  
572 algae and bedrock sample sites mentioned in the text. Onshore geology of this region  
573 modified from Garde and Steenfelt (1999a, b). Abbreviations used: M–metagreywacke;  
574 B–basalt, G–Gneiss; Q–Qeqertarsuaq algae; K–Karratfjord algae; V–Vaigat algae. **(B)**  
575 Map showing ocean currents of Greenland and the study area of Disko Bugt (box in black  
576 outline). The inset map shows the location of Disko Bugt (box in black outline) and core  
577 DA04-31T. Abbreviations used; EGC–East Greenland Current (blue); WGC–West  
578 Greenland Current (red).

579 **Figure 2.** Compilation of Os isotope ( $^{187}\text{Os}/^{188}\text{Os}$ ) values of lithological samples  
580 (abbreviations are as in Figure 1A), algae samples (additional abbreviations are; 5, 8 and  
581 30–Station 5, 8 and 30, respectively) and shallow (2-4 cm below seafloor) sediment  
582 samples. Algae samples are taken from within the water column. Uncertainties on Os  
583 isotopes are  $2\sigma$  and are smaller than all data points. See text for full details of algae  
584 locations and discussion.

585 **Figure 3.** Profiles of sediment samples and cores. **(A)**  $^{187}\text{Os}/^{188}\text{Os}$  record of core DA00-  
586 06 over past *c.* 9 ka cal. BP with four stages of ice sheet advance and retreat recorded in  
587 the core. Panel on the right displays foraminifera frequencies of glaciomarine and  
588 Atlantic water species expressed as a % of total specimens counted (from Lloyd et al.,  
589 2005); **(B)**  $^{187}\text{Os}/^{188}\text{Os}$  record of core MSM-520 over past 11.4 ka cal. BP. Panel on the  
590 right displays foraminifera frequencies of Atlantic water species expressed as a

591 percentage of total specimens counted (from McCarthy, 2011); (C) Profile of depth  
592 against  $^{187}\text{Os}/^{188}\text{Os}$  for core DA04-31T over the past c. 10 ka cal. BP. Uncertainties on Os  
593 isotopes are  $2\sigma$  and are smaller than all data points. See text for full details.

594 **Figure 4.** Simple mixing diagram of Osmium isotope composition of sediment and  
595 macro-algae samples plotted against  $1/^{192}\text{Os}$  to highlight trends in physical mixing of the  
596 Disko Bugt region water bodies and related samples. Macro-algae samples do not fit with  
597 general mixing trend observed in core samples. Data for basalt / picrite is sample 7712  
598 (their most radiogenic sample) from Schaefer et al. (2000) with  $^{192}\text{Os}$  calculated based on  
599 a natural abundance of 40.78%. The highly radiogenic Archean gneiss sample ( $1/^{192}\text{Os}$   
600  $>2$ ) is not plotted. GoM algae-Gulf of Mexico macro-algae. See text for further  
601 discussion.

602

## 603 **References**

604 Bronk Ramsey, C., 2009, Bayesian analysis of radiocarbon dates: *Radiocarbon*, **51**, 337-  
605 360

606 Burton, K.W., Gannoun, A., and Parkinson, I.J., 2010, Climate driven glacial-interglacial  
607 variations in the osmium isotope composition of seawater recorded by planktonic  
608 foraminifera: *Earth and Planetary Science Letters*, **295**, 58-68  
609 doi.org/10.1016/j.epsl.2010.03.026.

610 Carlson, A.E., and Winsor, K., 2012, Northern Hemisphere ice-sheet responses to past  
611 climate warming: *Nature Geosciences*, **5**, 607-613. DOI: 10.1038/NGEO1528

612 Christoffersen, P., and Hambrey, M. J., 2006, Is the Greenland Ice Sheet in a state of  
613 collapse?: *Geology Today*, **22**, 98-103. doi.org/10.1111/j.1365-2451.2006.00561.x.

614 Colville, E. J., Carlson, A. E., Beard, B. L., Hatfield, R. G., Stoner, J. S., Reyes, A. V.,  
615 and Ullman, D. J. 2011, Sr-Nd-Pb isotope evidence for ice-sheet presence on southern  
616 Greenland during the Last Interglacial: *Science*, **333**, 620-623.

617 Cumming, V.M., Poulton, S.W., Rooney, A.D., and Selby, D., 2013, Anoxia in the  
618 terrestrial environment during the Late Mesoproterozoic: *Geology*, **41**, 583-586.

619 Du Vivier, A.D.C., Selby, D., Sageman, B.B., Jarvis, I., Grocke, D.R., Silke, V., 2013.  
620 Marine  $^{187}\text{Os}/^{188}\text{Os}$  isotope stratigraphy reveals the interaction of volcanism and ocean

621 circulation during Oceanic Anoxic Event 2: *Earth and Planetary Science Letters*, **389**,  
622 23-33.

623 Du Vivier, A.D.C., Selby, D., Condon, D.J., Takashima, R., Nishi, H., 2015. Pacific  
624  $^{187}\text{Os}/^{188}\text{Os}$  isotope chemistry and U-Pb geochronology: synchronicity of global Os  
625 isotope change across OAE 2: *Earth and Planetary Science Letters*, *in press*.

626 Dalai, T.K., Suzuki, K., Minagawa, M., and Nozaki, Y., 2005, Variations in seawater  
627 osmium isotope composition since the last glacial maximum: a case study from the Japan  
628 Sea: *Chemical Geology*, **232**, 87-98. doi.org/10.1016/j.chemgeo.2005.04.012.

629 Dalai, T.K., and Ravizza, G., 2006, Evolution of osmium isotopes and iridium as  
630 paleoflux tracers in pelagic carbonates: *Geochimica et Cosmochimica Acta*, **70**, 3928-  
631 3942.

632 Engleman, E. E., Jackson, L. L., Norton, D. R., and Fischer, A. G., 1985, Determination  
633 of carbonate carbon in geological materials by coulometric titration: *Chemical Geology*,  
634 **53**, 125-128.

635 Farmer, G. L., Barber, D., & Andrews, J., 2003, Provenance of Late Quaternary ice-  
636 proximal sediments in the North Atlantic: Nd, Sr and Pb isotopic evidence: *Earth and*  
637 *Planetary Science Letters*, **209**, 227-243.

638 Flowerdew, M.J., Tyrell, S., and Peck, V.L., 2013, Inferring sites of subglacial erosion  
639 using the Pb isotopic composition of ice-rafted feldspar: Examples from the Weddell Sea,  
640 Antarctica: *Geology*, **41**, 147-150.

641 Funder, S., Kjellerup, K., Kjær, K.H., and Ó Cofaigh, C., 2011, The Greenland ice sheet  
642 during the last 300,000 years: A review, *in* Ehlers, J., Gibbard, P., and Hughes, P.D., eds.,  
643 Quaternary Glaciations—Extent and Chronology: A Closer Look: *Developments in*  
644 *Quaternary Science*, **15**, 699–713, doi:10.1016/B978-0-444-53447-7.00050-7.

645 Garde, A.A., and Steenfelt, A., 1999a, Precambrian geology of Nuussuaq and the area  
646 north-east of Disko Bugt, West Greenland. In: Kalsbeek, F. (ed.), Precambrian geology of  
647 the Disko Bugt region, West Greenland. Copenhagen: GEUS, pp. 6-40.

648 Garde, A.A., Steenfelt, A., 1999b, Proterozoic tectonic overprinting of Archean gneisses  
649 in Nuussuaq, West Greenland. In: Kalsbeek, F. (ed.), Precambrian geology of the Disko  
650 Bugt region, West Greenland. Copenhagen: GEUS, pp. 141-154.

651 Goodrich, C.A., and Patchett, P.J., 1991, Nd and Sr isotope chemistry of metallic iron-  
652 bearing, sediment contaminated Tertiary volcanics from Disko Island, Greenland: *Lithos*,  
653 **27**, 13-27. doi.org/10.1016/0024-4937(91)90017-F.

654 Gregory, J. M., Huybrechts, P., and Raper, S. C., 2004. Climatology: Threatened loss of  
655 the Greenland ice-sheet: *Nature*, **428**, 616-616.

656 Harris, N. B., Mnich, C. A., Selby, D., and Korn, D., 2013, Minor and trace element and  
657 Re–Os chemistry of the Upper Devonian Woodford Shale, Permian Basin, west Texas:  
658 Insights into metal abundance and basin processes: *Chemical Geology*, **356**, 76-93.

659 Hogan, K., Dix, J., Lloyd, J., Long, A., Cotterill, C., 2011, Near surface stratigraphy of  
660 eastern Disko Bugt, West Greenland: implications for glacial marine sedimentation: *Journal*  
661 *of Quaternary Science*, **26**, 757-766. doi/org. 10.1002/jqs.1500

662 Holland, D. M., Thomas, R. H., de Young, B., Ribergaard, M. H., and Lyberth, B., 2008,  
663 Acceleration of Jakobshavn Isbræ triggered by warm subsurface ocean waters: *Nature*  
664 *Geoscience*, **1**, 659–664,

665 Howat, I.M., Joughin, I.R., and Scambos T.A., 2007, Rapid changes in ice discharge  
666 from Greenland outlet glaciers: *Science*, **315**, 1559–1561 doi: 10.1126/science.1138478.

667 Huffman, E.W.D., 1977, Performance of a new automatic carbon dioxide coulometer,  
668 *Microchemical Journal*, **22**, 567-573.

669 Jennings, A.E., Walton, M.E., O’Cofaigh, C., Kilfeather, A., Andrews, J.T., Ortiz, J.D.,  
670 De Vernal, A., and Dowdeswell, J.A. 2014. Paleoenvironments during Younger Dryas-  
671 Early Holocene retreat of the Greenland Ice Sheet from outer Disko Trough, central west  
672 Greenland: *Journal of Quaternary Science* **29**, 27 – 40

673 Jonkers, L., Zahn, R., Thomas, A., Henderson, G., Abouchami, W., François, R., and  
674 Bickert, T., 2015, Deep circulation changes in the central South Atlantic during the past  
675 145 kyrs reflected in a combined  $^{231}\text{Pa}/^{230}\text{Th}$ , Neodymium isotope and benthic record:  
676 *Earth and Planetary Science Letters*, **419**, 14-21.

677 Joughin, I., Abdalati, W., and Fahnestock, M.A., 2004, Large fluctuation in speed of  
678 Jakobshavn Isbræ, Greenland: *Nature*, **432**, 608-610. doi.org/10.1038/nature03130.

679 Kalsbeek, F., Pulvertaft, T.C.R., and Nutman, A.P., 1998, Geochemistry, age and origin  
680 of metagreywackes from the Palaeoproterozoic Karrat Group, Rinkian Belt, West

681 Greenland: *Precambrian Research*, **91**, 383-399. doi.org/10.1016/S0301-9268(98)00059-  
682 X.

683 Kendall, B.S., Creaser, R.A., Ross, G.M., and Selby, D., 2004, Constraints on the timing  
684 of Marinoan ‘Snowball Earth’ glaciation by  $^{187}\text{Re}/^{187}\text{Os}$  dating of a Neoproterozoic post-  
685 glacial black shale in Western Canada: *Earth and Planetary Science Letters*, **222**, 729-  
686 740. doi.org/10.1016/j.epsl.2004.04.004.

687 Kendall, B.S., van Acken, D., Creaser, R.A., 2013, Depositional age of the early  
688 Paleoproterozoic Klipputs Member, Nelani Formation (Ghaap Group, Transvaal  
689 Supergroup, South Africa) and implication for low-level Re-Os geochronology and  
690 Paleoproterozoic global correlations. *Precambrian Research*, **237**, 1-12.

691 Khan, S. A., Aschwanden, A., Bjørk, A. A., Wahr, J., Kjeldsen, K. K., and Kjær, K. H.,  
692 2015. Greenland ice sheet mass balance: a review: *Reports on Progress in Physics*, **78**(4),  
693 046801

694 Knutz, P.C., Sicre, M.-A., Ebbesen, H., Christiansen, S., and Kuijpers, A., 2011,  
695 Multiple-stage deglacial retreat of the southern Greenland Ice Sheet linked with Irminger  
696 Current warm water transport: *Paleoceanography*, **26**, PA3204,  
697 doi:10.1029/2010PA002053.

698 Lane, T.P., Roberts, D.H., Rea, B.R., Rodés, A., Ó Cofaigh, C. and Vieli, A., 2014, Ice  
699 stream dynamics in the northern sector of the Uummannaq Ice Stream System, West  
700 Greenland: *Quaternary Science Reviews* **231**, 301-313.

701 Levasseur, S., Birck, J-L., and Allégre, C.J., 1998, Direct measurement of femtomoles of  
702 osmium and the  $^{187}\text{Os}/^{188}\text{Os}$  ratio in seawater: *Science*, **282**, 272-274.  
703 doi.org/10.1126/science.282.5387.272.

704 Levasseur, S., Birck, J-L., and Allégre, C.J., 1999, The osmium riverine flux and the  
705 oceanic mass balance of osmium: *Earth and Planetary Science Letters*, **174**, 7-23.  
706 doi.org/10.1016/S0012-821X(99)00259-9.

707 Long, A.J., Roberts, D.H., and Dawson, S., 2006, Early Holocene history of the west  
708 Greenland Ice Sheet and the GH-8.2 event: *Quaternary Science Reviews*, **25**, 904-922.

709 Long, A.J., and Roberts, D.H., 2003, Late Weichselian deglacial history of Disko Bugt,  
710 West Greenland, and the dynamics of Jakobshavns Isbrase ice stream: *Boreas*. **32**, 208-  
711 226.

712 Lloyd, J.M., Park, L.A., Kuijpers, A., and Moros, M, 2005, Early Holocene  
713 palaeoceanography and deglacial chronology of Disko Bugt, West Greenland:  
714 *Quaternary Science Reviews*, **24**, 1741-1755. doi.org/10.1016/j.quascirev.2004.07.024.

715 Ludwig, K.R., 1980, Calculation of uncertainties of U–Pb isotope data: *Earth and*  
716 *Planetary Science Letters*, **46**, 212–220

717 McCarthy, D.J., 2011, Late Quaternary ice-ocean interactions in central West Greenland,  
718 [PhD thesis]: Durham University, pp. 309.

719 McManus, J. F., Francois, R., Gherardi, J. M., Keigwin, L. D., and Brown-Leger, S.,  
720 2004. Collapse and rapid resumption of Atlantic meridional circulation linked to  
721 deglacial climate changes: *Nature*, **428**, 834-837.

722 Ó Cofaigh, C., J.A. Dowdeswell, A.E. Jennings, K.A. Hogan, A.A. Kilfeather, J.F.  
723 Hiemstra, R. Noormets, J. Evans, D.J. McCarthy, J.T. Andrews, J.M. Lloyd and M.  
724 Moros. 2013. An extensive and dynamic ice sheet on the West Greenland shelf during the  
725 last glacial cycle: *Geology*, **41**, 219-222. DOI: 10.1130/G33759.1

726 Nick, F. M., Vieli, A., Howat, I. M., and Joughin, I., 2009, Large-scale changes in  
727 Greenland outlet glacier dynamics triggered at the terminus: *Nature Geosciences*, **2**, 110–  
728 114, doi:10.1038/ngeo394.

729 Oxburgh, R., 1998, Variations in the osmium isotope composition of sea water of the past  
730 200, 000 years: *Earth and Planetary Science Letters*, **159**, 183-191.  
731 doi.org/10.1016/j.epsl.2007.08.033.

732 Oxburgh, R., 2001, Residence time of osmium in the oceans: *Geochemistry, Geophysics,*  
733 *Geosystems*, **2**, paper number 2000GC000104.

734 Oxburgh, R., Pierson-Wickman, A.-C., Reisberg, L., and Hemming, S., 2007, Climate  
735 correlated variations in seawater  $^{187}\text{Os}/^{188}\text{Os}$  over the past 200, 000 yr: evidence from the  
736 Cariaco Basin, Venezuela: *Earth and Planetary Science Letters*, **263**, 246-258.  
737 doi.org/10.1016/j.epsl.2007.08.033.

738 Paquay, F.S., Goderis, S., Ravizza, G., Vanhaecke, F., Boyd, M., Surovell, T.A., Holliday,  
739 V., Haynes, Jr, C.V., and Claeys, P., 2009, Absence of geochemical evidence for an  
740 impact event at the Bøllering-Allerød/Younger Dryas transition: *Proceedings of the*  
741 *National Academy of Sciences*, **106**, 21505-21510.



742 Paquay, F.S., and Ravizza, G., 2012, Heterogeneous seawater  $^{187}\text{Os}/^{188}\text{Os}$  during the Late  
743 Pleistocene glaciations: *Earth and Planetary Science Letters*, **349**, 126-138.  
744 doi.org/10.1016/j.epsl.2012.06.051.

745 Peucker-Ehrenbrink, B., and Ravizza, G., 2000, The marine osmium isotope record:  
746 *Terra Nova*, **12**, 205-219. doi.org/10.1046/j.1365-3121.2000.00295.x.

747 Peucker-Ehrenbrink, B., and Ravizza, G., 2012. Osmium isotope stratigraphy, in:  
748 Gradstein, F. M., Ogg, G., & Schmitz, M. (Eds.), The Geological Time Scale 2 volume  
749 set. Elsevier, Amsterdam, pp. 145-166.

750 Pfeffer, W.T., Harper, J.T., and O'Neel, S., 2008, Kinematic constraints on glacier  
751 contributions to 21<sup>st</sup>-Century Sea-Level Rise: *Science*, **321**, 1340-1343.  
752 doi.org/10.1126/science.1159099.

753 Prouty, N.G., Roark, E.B., Koenig, A.E., Demopoulos, A.W.J., Batista, F.C., Kocar, B.D.,  
754 Selby, D., McCarthy, M.D., and Mienis, F. Deep-sea coral record of human impact on  
755 watershed quality in the Mississippi River Basin: *Global Biogeochemical Cycles*, **28**, 29-  
756 43. doi: 10.1002/2013GB004754

757 Raiswell, R., Tranter, M., Benning, L. G., Siegert, M., De'ath, R., Huybrechts, P., and  
758 Payne, T., 2006. Contributions from glacially derived sediment to the global iron  
759 (oxyhydr) oxide cycle: implications for iron delivery to the oceans: *Geochimica et*  
760 *Cosmochimica Acta*, **70**, 2765-2780.

761 Ravizza, G., and Peucker-Ehrenbrink, B., 2003, The marine  $^{187}\text{Os}/^{188}\text{Os}$  record of the  
762 Eocene-Oligocene transition: the interplay of weathering and glaciation: *Earth and*  
763 *Planetary Science Letters*, **210**, 151-165. doi.org/10.1016/S0012-821X(03)00137-7.

764 Rignot, E., and Kanagaratnam, P., 2006, Changes in the velocity structure of the  
765 Greenland Ice Sheet: *Science*, **311**, 986–990 (doi: 10.1126/science.1121381).

766 Roberts, D.H., Rea, B.R., Lane, T.P., Schnabel, C., and Rodés, A., 2013, New constraints  
767 on Greenland ice sheet dynamics during the LGM: evidence from the Uummannaq ice  
768 stream system: *Journal of Geophysical Research*, doi:10.1002/jgrf20032.

769 Rooney, A.D., Selby, D., Houzay, J.-P., and Renne, P.R., 2010, Re-Os geochronology of  
770 a Mesoproterozoic sedimentary succession, Taoudeni basin Mauritania: implications for  
771 basin-wide correlations and Re-Os organic-rich systematics: *Earth and Planetary Science*  
772 *Letters*, **289**, 486-496. doi.org/10.1016/j.epsl.2009.11.039.

773 Rooney, A.D., Chew, D.M., and Selby, D., 2011, Re-Os geochronology of the  
774 Neoproterozoic-Cambrian Dalradian Supergroup of Scotland and Ireland: Implications  
775 for Neoproterozoic stratigraphy, glaciations and Re-Os systematics: *Precambrian*  
776 *Research*, **185**, 202-214, doi:10.1016/j.precamres.2011.01.009.

777 Rooney, A.D., Macdonald, F.A., Strauss, J.V., Dudas, F.Ö., Hallmann, C., 2014, Selby,  
778 D., Weathering the Snowball: *Proceedings of the National Academy of Sciences*, **111**, 51-  
779 56.

780 Schaefer, B.F., Parkinson, I.J., and Hawkesworth, C.J., 2000, Deep mantle plume  
781 osmium isotope signature from West Greenland Tertiary picrites: *Earth and Planetary*  
782 *Science Letters*, **175**, 105-118. doi.org/10.1016/S0012-821X(99)00290-3.

783 Selby, D., and Creaser, R.A., 2003, Re-Os geochronology of organic-rich sediments: an  
784 evaluation of organic matter analysis methods: *Chemical Geology*, **200**, 225-240.  
785 doi.org/10.1016/S0009-2541(03)00199-2.

786 Selby, D., 2007, Direct Rhenium-Osmium age of the Oxfordian-Kimmeridgian boundary,  
787 Staffin bay, Isle of Skye, U.K., and the late Jurassic time scale: *Norwegian Journal of*  
788 *Geology*, **87**, 291-299.

789 Selby, D., Creaser, R.A., Stein, H.J., Markey, R.J., and Hannah, J.L., 2007, Assessment  
790 of the <sup>187</sup>Re decay constant by cross calibration of Re-Os in molybdenite and U-Pb zircon  
791 chronometers in magmatic ore systems: *Geochimica et Cosmochimica Acta*, **71**, 1999-  
792 2019. doi.org/10.1016/j.gca.2007.01.008

793 Sharma, M., Papanastassiou, D.A., and Wasserburg, G.J., 1997, The concentration and  
794 isotopic composition of osmium in the oceans: *Geochimica et Cosmochimica Acta*, **61**,  
795 3287-3299. doi.org/10.1016/S0016-7037(97)00210-X.

796 Straneo, F., et al., 2013, Challenges to understanding the dynamic response of  
797 Greenland's marine terminating glaciers to oceanic and atmospheric forcing: *Bulletin*  
798 *American Meteorological Society*, **94**, 1131-1144.

799 Williams, G.A., and Turekian, K.K., 2004, The glacial-interglacial variation of seawater  
800 osmium isotopes as recorded in Santa Barbara Basin: *Earth and Planetary Science*  
801 *Letters*, **228**, 379-389. doi.org/10.1016/j.epsl.2004.10.004.

802 Woodhouse, O.B, Ravizza, G., Kenison Falkner, K., Statham, P.J., and Peucker-  
803 Ehrenbrink, B., 1999. Osmium in seawater: vertical profiles of concentration and isotopic

804 composition in the eastern Pacific Ocean: *Earth and Planetary Science Letters*, **183**, 223-  
805 233.

806 Ulff-Møller, F., 1990, Formation of native iron in sediment-contaminated magma: I. A  
807 case study of the Hanekammen Complex on Disko Island, West Greenland: *Geochimica*  
808 *et Cosmochimica Acta*, **54**, 57-70. doi.org/10.1016/0016-7037(90)90195-Q.

809 Yang, J.S., 1991 High rhenium enrichment in brown algae: a biological sink of rhenium  
810 in the sea?: *Hydrobiologia*, **211**, 165-170.

811 Young, N.E., Briner, J.P., Axford, Y., Csatho, B., Babonis, G.S., Rood, D.H., Finkel, C.,  
812 2011, Response of a marine-terminating Greenland outlet glacier to abrupt cooling 8200  
813 and 9300 years ago: *Geophysics Research Letters*, **38**, L24701.  
814 <http://dx.doi.org/10.1029/2011GL049639>.

815 Young, N.E., Briner, J.P., Rood, D.H., Finkel, R.C., Corbett, L.B., Bierman, P.R., 2013,  
816 Age of the Fjord Stade moraines in the Disko Bugt region, western Greenland, and the  
817 9.3 and 8.2 ka cooling events: *Quaternary Science Reviews*, **60**, 76e90.  
818 <http://dx.doi.org/10.1016/j.quascirev.2012.09.028>.

Table 1: Sampling details for all cores and samples.

Sample and depth	Core length (cm)	Water depth (m)	sedimentation rates (mm/yr)	Re range (ng/g)	Os range (pg/g)	Foraminifera species
DA04-31T	72	2525	0.02 - 0.16*	1.3 - 12	37 - 70	N-D
DA00-06	960	363	13 - 0.24	0.4 - 26	42 - 103	N-D
MSM-520	1200	545.7 <sup>#</sup>	0.9	4 - 18	86 - 213	Lower sections: <i>Elphidium excavatum f. clavata</i> Upper sections: <i>Trochammina nana</i>

\* Knutz et al., (2011)

<sup>#</sup> McCarthy, (2011)

Table 1: Re and Os elemental and isotopic composition data, calibrated ages and samples locations for surface samples and seaweed.

	w.t% TOC	% CaCO <sub>3</sub>	Re (ng/g)	±	Os (pg/g)	±	<sup>182</sup> Os (pg/g)	±	<sup>182</sup> Os%	<sup>187</sup> Re / <sup>188</sup> Os	±	<sup>187</sup> Os / <sup>188</sup> Os	±	rho <sup>a</sup>	Os <sub>i</sub> <sup>b</sup>	±	Age cal. Kyr	Lat and long	Water depth (m)
<b>Surface spot samples</b>																			
MSM-340	1.77	1.24	6.37	0.021	118.2	0.8	43.2	0.2	36.5	293.7	2.7	1.13	0.01	0.65	1.13	0.01	0.01	68°36'55"N, 55°19'59"W	ND
MSM-380	ND	ND	1.65	0.005	126.7	0.6	50.0	0.2	39.5	65.6	0.6	0.48	0.01	0.65	0.48	0.01	0	70°19'04"N, 53°41'09"W	ND
MSM 380 r	ND	ND	1.57	0.0051	117.7	2.2	46.4	0.9	37.2	67.3	2.7	0.50	0.03	0.70	0.50	0.02	-	-	ND
MSM-540	ND	ND	1.36	0.004	353.5	2.2	131.4	0.5	39.4	20.5	0.2	0.98	0.01	0.65	0.98	0.01	0	69°38'06"N, 57°26'03"W	ND
Site 4	0.14	0.59	1.94	0.019	36.5	0.4	11.4	0.1	31.2	339.3	6.7	2.62	0.05	0.76	2.62	0.04	0	69°08'00"N, 51°24'05"W	ND
<b>Seaweed (Greenland)</b>																			
Qeqertarsuaq ( <i>Ascophyllum nodosum</i> )	ND	ND	22.01	0.09	12.6	0.7	4.7	0.3	37.2	9368.4	1194.1	0.96	0.13	0.95	0.96	0.13	<5yr	69°14'51"N, 53°32'20"W	0
Vaigat ( <i>Laminaria digitata</i> )	ND	ND	1.26	0.0297	14.1	0.7	5.3	0.3	37.5	474.6	54.7	0.91	0.11	0.92	0.91	0.11	<5yr	70°02'04"N, 52°55'44"W	0
Karratfjord ( <i>Fucus distichus</i> )	ND	ND	15.29	0.06	14.0	0.7	4.7	0.3	33.6	6459.5	791.9	1.89	0.24	0.99	1.89	0.24	<5yr	71°32'09"N, 53°12'34"W	0
<b>Lithologies</b>																			
KA14 Metagreywacke	ND	ND	0.04	0.000*	85.8	1.6	34.0	0.7	39.7	2.1	0.1	0.44	0.03	0.70	ND	ND	>1 Ga	71°31'30"N, 52°57'53"W	ND
ST24 Gneiss	ND	ND	0.00	0.000*	1.6	0.0*	0.5	0.0*	30.5	17.7	0.8	2.82	0.16	0.69	ND	ND	>2 Ga	70°40'05"N, 51°33'08"W	ND
Basalt	ND	ND	0.17	0.006	19.9	0.3	7.1	0.1	35.8	46.2	2.0	1.31	0.04	0.47	ND	ND	>50 Ma	71°31'01"N, 55°17'29"W	ND
Basalt r	ND	ND	0.17	0.006	18.1	0.3	6.4	0.1	35.6	53.6	2.4	1.36	0.05	0.50	ND	ND	-	-	ND
<b>Core open ocean samples</b>																			
<b>Core SO93 - Laccadive Sea</b>																			
01KL: 0-9 cm	3.19	44.38	16.20	0.05	179.5	0.8	66.1	0.2	36.8	487.5	2.9	1.06	0.01	0.59	1.06	0.01	0.1	07°04'36"N, 79°26'53"E	1688
01KL: 93-100 cm	1.45	46.30	13.87	0.05	130.1	0.6	47.9	0.1	36.8	576.5	3.6	1.06	0.01	0.58	1.06	0.01	9.5	-	-
<b>Core SO 189 - Mentawai Strait</b>																			
39KL: 0-6 cm	2.21	19.76	7.79	0.03	215.8	1.3	79.8	0.3	37.0	194.1	1.6	1.02	0.01	0.64	1.02	0.01	0.5	00°47'40"S, 99°54'51"E	571
39KL: 343-348 cm	1.92	18.84	11.72	0.04	142.8	0.7	52.8	0.2	37.0	441.8	3.1	1.02	0.01	0.63	1.02	0.01	10	-	-
<b>Core SO 161 - Pacific Ocean</b>																			
22SL: 0-6 cm	2.17	0.52	12.39	0.04	174.5	0.8	64.3	0.2	36.9	383.5	2.3	1.05	0.01	0.57	1.05	0.01	0.5	36°13'16"S, 73°40'50"W	1001
22SL: 250-255 cm	1.54	1.97	16.36	0.05	111.6	0.5	41.2	0.1	36.9	790.6	4.5	1.04	0.01	0.58	1.04	0.01	9.9	-	-
<b>Open Gulf of Mexico seaweed</b>																			
Station 5 ( <i>Sargassum fluitans &amp; natans</i> )	ND	ND	0.27	0.03	67.9	0.9	25.0	0.6	36.8	21.1	2.3	1.06	0.03	0.19	1.06	0.03	<5yr	26°00'07"N, 91°28'04"W	ND
Station 8 ( <i>Sargassum natans</i> )	ND	ND	0.16	0.03	78.5	0.9	28.9	0.7	36.8	10.9	2.1	1.05	0.03	0.10	1.05	0.03	<5yr	26°00'25"N, 91°04'05"W	ND
Station 30 ( <i>Sargassum natans</i> )	ND	ND	0.08	0.0516	61.2	1.4	22.6	1.1	36.9	6.8	4.6	1.03	0.06	0.07	1.03	0.06	<5yr	26°00'01"N, 88°08'13"W	ND

r indicates repeat analysis

\*indicates uncertainty is less than significant figures stated

<sup>a</sup> rho is the associated error correlation function (Ludwig, 1980).<sup>b</sup> Os<sub>i</sub> values have been calculated at the deposition age of the sediment e.g., 8.7 ka cal. BP.

ND Not determined

Table 2: Sampling details for all cores and samples.

Sample and depth	Core length (cm)	Water depth (m)	Sedimentation rates (mm/yr)	Re range (ng/g)	Os range (pg/g)	Foraminifera species
DA04-31T	72	2525	0.02 - 0.16*	1.3 - 12	37 - 70	N-D
DA00-06	960	363	13 - 0.24	0.4 - 26	42 - 103	N-D
MSM-520	1200	545.7 <sup>#</sup>	0.9	4 - 18	86 - 213	Lower sections: <i>Elphidium excavatum f. clavata</i> Upper sections: <i>Trochammina nana</i>

\* Knutz et al., (2011)

<sup>#</sup> McCarthy, (2011)

Table 3: Radiocarbon dates from analysed cores.

Core	Depth (cm)	Lab Code	Material	<sup>14</sup> C age (yr BP)	Mean calibrated age (yr BP)	Age range 2σ (yr BP)
MSM-520	41	Poz-22364	Shell	1205 ± 30	744	831 - 666
	161	Poz-22365	Shell	2260 ± 30	1867	1963 - 1780
	216 - 218	LuS 8601	Benthic foraminifera	3055 ± 60	2836	2980 - 2714
	328-330	LuS 8550	Benthic foraminifera	4730 ± 70	4995	5220 - 4821
	452 - 456	LuS 8549	Benthic foraminifera	6125 ± 65	6555	6713 - 6400
	480	AAR-11700	Bivalve	6326 ± 43	6790	6906 - 6668
	556 - 560	LuS 8548	Benthic foraminifera	7065 ± 70	7547	7666 - 7424
	640 - 642	Poz-30962	Bivalve	7900 ± 40	8364	8457 - 8279
	692 - 694	LuS 8547	Benthic foraminifera	8340 ± 70	8896	9106 - 8655
896 - 906	LuS 7707	Benthic foraminifera	9970 ± 100	10908	11158 - 10630	
DA00-06	5-7	KIA-17925	Benthic foraminifera	1500 ± 90	1047	943 - 1160
	72-76	B203723	Benthic foraminifera	6300 ± 40	6762	6653 - 6872
	159	AAR-6837	Shell	7350 ± 68	7791	7663 - 7937
	426-434	KIA-23024	Benthic foraminifera	7270 ± 45	7713	7640 - 7816
	646-654	KIA-23025	Benthic foraminifera	7430 ± 70	7889	7734 - 8018
	891	AAR-6839	Shell	7843 ± 72	8321	8154 - 8416

Using OxCal v4.1 (Bronk Ramsey, 2009)

<sup>14</sup>C Age (uncorrected), 100% marine, Marine09curve, Delta R = 0±0

MSM-520 chronology from McCarthy (2011)

DA00-06 chronology from Lloyd et al. (2005) and Hogan et al. (2011)

Table 4: Re and Os elemental and isotopic composition data, calibrated ages and sample location details for core sections.

	wt.% TOC	% CaCO <sub>3</sub>	Re (ng/g)	±	Os (pg/g)	±	<sup>192</sup> Os (pg/g)	±	<sup>192</sup> Os%	<sup>187</sup> Re / <sup>188</sup> Os	±	<sup>187</sup> Os / <sup>188</sup> Os	±	rho <sup>a</sup>	Osi <sup>b</sup>	±	Age cal. Kyr <sup>c</sup>	Lat and Long	water depth (m)	
<b>Core DA00-06 (proximal to Jakobshavn Isbræ)</b>																				
8-16	0.78	0.65	13.90	0.04	71.6	1.5	24.9	0.5	34.8	1109.0	44.7	1.55	0.09	0.71	1.55	0.05	1.50	69°10'21"N, 51°23'71"W	363	
32-40	0.81	0.47	25.71	0.08	80.7	1.7	28.8	0.6	35.6	90.0	3.6	1.34	0.08	0.71	1.34	0.05	3.50			
56-64	0.66	0.85	2.63	0.01	95.6	1.2	33.4	0.3	34.9	156.9	3.2	1.53	0.04	0.70	1.53	0.03	5.60			
80-88	0.56	0.77	13.72	0.04	80.2	1.7	28.4	0.6	35.4	962.0	38.7	1.40	0.08	0.71	1.40	0.05	6.85			
80-88 r	as above	as above	13.21	0.04	76.6	1.6	27.0	0.5	35.2	974.0	39.1	1.44	0.08	0.70	1.44	0.05	6.85			
104-112	0.31	1.14	9.33	0.03	79.4	1.7	27.7	0.6	34.8	670.4	27.0	1.54	0.09	0.71	1.54	0.05	7.12			
152-160	0.16	0.98	2.80	0.01	54.7	1.2	17.8	0.4	32.5	313.7	12.6	2.19	0.12	0.71	2.19	0.08	7.63			
248-256	0.05	1.17	0.62	0.00	53.4	1.2	17.7	0.4	35.4	69.6	2.8	2.02	0.11	0.71	2.02	0.07	7.71			
344-352	0.04	1.12	0.46	0.00	65.7	1.5	21.6	0.4	33.0	42.7	1.7	2.08	0.12	0.71	2.08	0.07	7.77			
344-352 r	as above	as above	0.50	0.00	65.0	1.5	21.5	0.4	32.9	46.2	1.9	2.06	0.12	0.71	2.06	0.07	7.77			
440-448	0.05	1.16	0.49	0.00	62.8	1.3	21.6	0.4	34.4	44.9	1.8	1.66	0.09	0.71	1.66	0.06	7.83			
560-568	0.12	0.47	0.78	0.00	102.7	2.2	35.2	0.7	34.2	43.9	1.8	1.71	0.10	0.70	1.71	0.06	7.96			
640-648	0.10	0.52	0.86	0.00	65.6	1.4	22.5	0.5	34.3	75.6	3.0	1.68	0.10	0.71	1.68	0.06	8.05			
752-760	0.02	1.23	0.39	0.00	56.2	1.3	18.2	0.4	32.4	42.6	1.7	2.22	0.13	0.71	2.22	0.08	8.17			
848-856	0.03	1.21	0.40	0.00	42.3	1.0	13.6	0.3	32.2	58.5	2.4	2.29	0.13	0.71	2.29	0.08	8.28			
940-944	0.07	1.11	0.47	0.00	46.3	1.1	14.7	0.3	31.8	63.8	2.6	2.41	0.14	0.71	2.41	0.08	9.0			
<b>MSM-520 (52m NW of the Nuussuaq Peninsula)</b>																				
4-14	1.52	0.34	7.18	0.036	180.2	1.0	68.3	0.3	37.9	209.2	1.9	0.81	0.01	0.57	0.81	0.01	0.33	70°48'57"N 56°50'53"W	546	
106-112	1.59	0.29	9.64	0.031	174.7	1.0	65.6	0.3	37.6	292.2	2.4	0.88	0.01	0.64	0.88	0.01	1.28			
210-216	1.63	0.32	12.56	0.041	212.9	1.2	80.8	0.3	38.0	309.2	2.4	0.80	0.01	0.62	0.80	0.01	2.66			
304-310	1.39	0.45	8.11	0.026	149.8	1.1	56.7	0.3	37.8	284.9	3.3	0.83	0.01	0.63	0.83	0.01	4.38			
306	1.41	0.38	5.81	0.019	144.1	1.2	55.2	0.7	38.3	209.5	2.9	0.73	0.01	0.69	0.73	0.01				
404-410	1.33	0.20	10.13	0.033	157.7	0.9	59.2	0.2	37.5	340.7	2.8	0.90	0.01	0.63	0.90	0.01	5.83			
504-510	1.35	0.40	17.55	0.057	137.4	0.9	51.4	0.2	37.4	679.5	6.3	0.93	0.01	0.64	0.93	0.01	6.98			
506	1.35	0.37	14.75	0.048	100.9	0.5	37.5	0.2	37.1	783.2	5.2	0.99	0.01	0.62	0.99	0.01				
604-610	1.16	0.38	9.70	0.031	113.2	0.7	41.5	0.2	36.7	464.9	4.3	1.09	0.01	0.65	1.09	0.01	7.98			
704-710	1.07	0.62	4.22	0.014	112.4	0.7	41.5	0.2	36.9	202.4	1.8	1.03	0.01	0.65	1.03	0.01	9.00			
800-806	0.97	0.53	8.24	0.027	86.1	0.6	31.5	0.2	36.6	520.4	5.5	1.11	0.02	0.67	1.11	0.01	10.00			
803	0.99	0.64	1.24	0.004	66.2	1.3	24.2	1.0	36.6	101.9	4.1	1.10	0.06	0.71	1.10	0.04				
903	0.86	1.02	1.68	0.005	86.8	1.7	32.2	0.6	37.1	104.1	4.2	1.00	0.06	0.71	1.00	0.03				
904-910	0.91	0.94	2.94	0.010	85.5	0.7	30.5	0.2	35.6	192.3	2.1	1.35	0.02	0.56	1.35	0.01	11.14			
<b>Core DA-04-31T (130m SW of Nuuk)</b>																				
0-2	0.35	11.66	9.58	0.01	52.0	0.3	19.2	0.1	37.0	990.6	8.7	1.01	0.01	0.66	1.01	0.01	0.14	62°33'78"N, 54°0'22"W	2525	
10-12	0.16	6.61	2.05	0.02	36.7	0.2	13.6	0.1	36.9	300.5	2.6	1.04	0.01	0.66	1.04	0.01	1.55			
20-22	0.16	11.33	1.31	0.02	54.9	0.3	20.6	0.1	37.6	126.7	1.1	0.88	0.01	0.65	0.88	0.01	2.96			
30-32	0.19	8.00	11.98	0.02	43.1	0.3	15.8	0.1	36.7	1504.4	14.9	1.07	0.01	0.65	1.07	0.01	4.37			
40-42	0.20	8.54	3.05	0.02	70.4	0.4	26.6	0.1	37.8	228.4	2.0	0.84	0.01	0.65	0.84	0.01	5.78			
50-52	0.24	3.03	5.61	0.02	44.5	0.3	16.1	0.1	36.2	691.1	6.0	1.19	0.01	0.66	1.19	0.01	7.19			
60-62	0.20	2.19	1.91	0.02	47.6	0.4	17.4	0.1	36.5	218.7	3.0	1.13	0.02	0.59	1.13	0.01	8.60			
70-72	0.07	1.32	1.35	0.01	41.4	0.3	15.4	0.1	37.1	174.6	1.5	0.98	0.01	0.66	0.98	0.01	10.01			

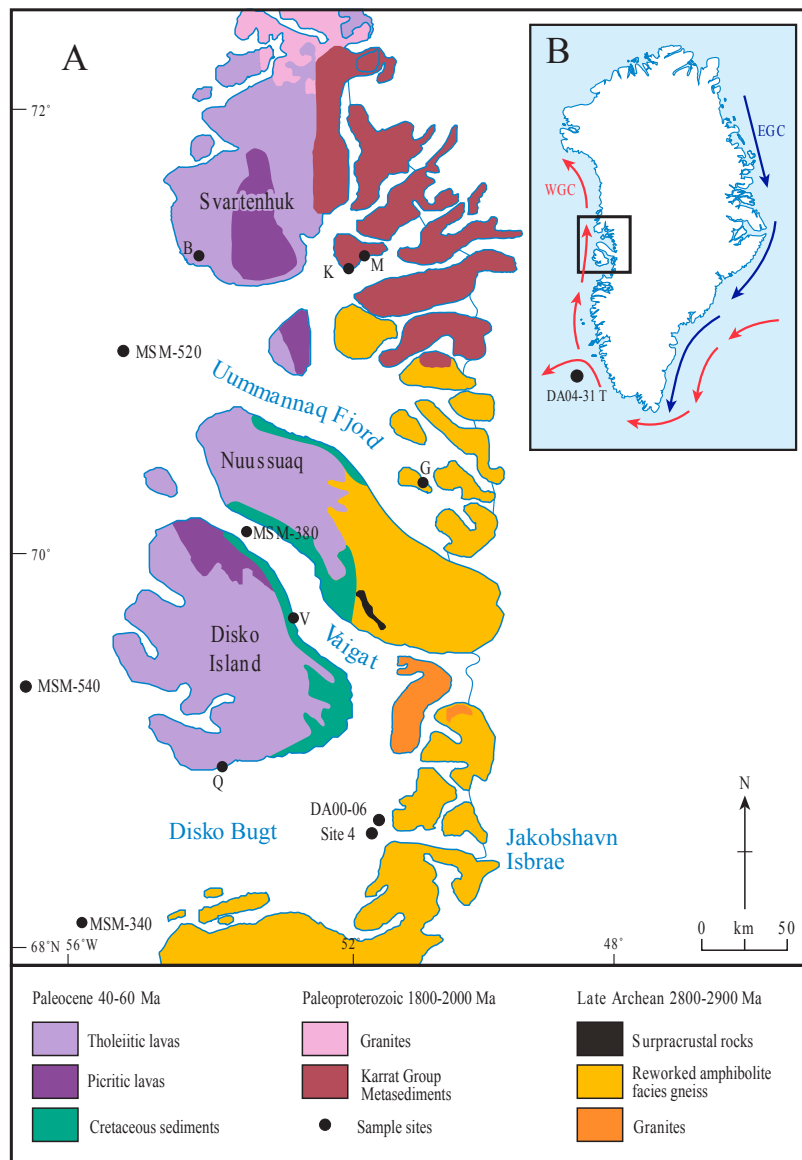
r indicates repeat analysis

<sup>a</sup>rho is the associated error correlation function (Ludwig, 1980).

<sup>b</sup>Osi values have been calculated at 10 ka. Calculated initials are identical to the modern dav values at the 2sf level.

<sup>c</sup>Calibrated ages for MSM-520 from McCarthy (2011), DA00-06 from Lloyd et al. (2005) and DA04-31T based on correlation from Knutz et al. (2011).





Surface and outcrop samples

$^{187}\text{Os}/^{188}\text{Os}$

0.0 0.2 0.4 0.8 1.0 1.2 1.4 1.6 1.8 2.0 2.2 2.4 2.6 2.8 3.0

